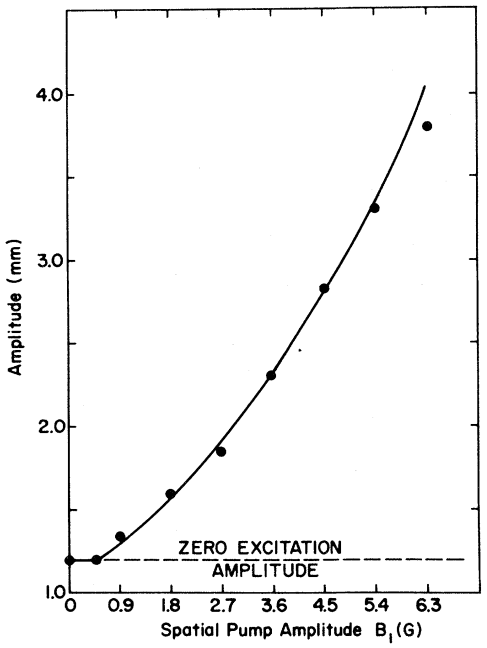

FIG. 4. Pumping for two pump periods off-resonance so that detuning effects are not important for a plasma with $\omega_p^2/\omega_{c0}^2 \simeq 0.14$, $\Omega_0 \simeq 5.6\times 10^8$ rad/sec, $\omega_0 \simeq 6.4\times 10^8$ rad/sec, and $B_0 \simeq 35$ G.

has been shown to be in agreement with Eq. (4).

The authors are grateful to Professor J. Guillory who suggested the possibility of parametric excitation of these modes. We also appreciate the helpful discussions with Professor D. Hammer, Professor H. Lashinsky, Professor C. Liu, and with Dr. D. Batchelor and Dr. J. VanZandt.

*This research was supported by the National Science Foundation under Grant No. PHY-7401056.

[1]R. A. Mahaffey, S. A. Goldstein, R. C. Davidson, and A. W. Trivelpiece, Phys. Rev. Lett. 35, 1439 (1975).

[2]A. J. Theiss, R. A. Mahaffey, and A. W. Trivelpiece, Phys. Rev. Lett. 35, 1436 (1975); A. J. Theiss, University of Maryland Technical Report No. 74-093, 1973 (unpublished).

[3]Herbert Lashinsky, "Analysis of Nonlinear Phenomena" (North-Holland, Amsterdam, to be published).

[4]R. C. Davidson, *Theory of Nonneutral Plasmas* (Benjamin, Reading, Mass., 1974).

Nonlinear Evolution of the Electron-Beam–Plasma Instability

H. Ikezi, R. P. H. Chang, and R. A. Stern
Bell Laboratories, Murray Hill, New Jersey 07974
(Received 28 October 1975)

Detailed experimental studies of the nonlinear evolution of an electron-beam–plasma instability reveal trapping of unstable electron-plasma waves by ion-acoustic modes as well as scattering of beam electrons.

Recent interests in heating plasmas by high-current relativistic electron beams[1] have led to the study of the parametric instabilities associated with large-amplitude waves excited by the electron-beam–plasma instability.[2] We report here several new nonlinear features of the beam-plasma instability. First, we show that the trapping of the electron-plasma wave by the ion-acoustic wave modifies the convective nature of the beam-plasma instability to a temporal instability. Secondly, we present evidence that the saturation mechanism, beam scattering by the wave, occurs via three-dimensional processes, in which wave propagation at an angle to the beam axis is essential.

The experiments are carried out in a double-plasma device,[3] consisting of two separately generated argon discharge plasmas contained in 30-cm-diam metal chambers connected by a fine metal mesh. A negative potential applied to the driver plasma with respect to the target plasma extracts an electron beam which penetrates the target plasma and fills it. Typical parameters of the argon plasmas are electron density $n_0 \sim 10^9$ cm^{-3}, temperature $T_e \simeq 3$ eV, background gas pressure 2×10^{-4} Torr, and beam density $n_b \lesssim 0.05 n_0$. The beam energy is varied up to 100 eV, with corresponding velocity u up to $8v_e$ (v_e is the electron thermal speed) and a beam thermal spread $v_b < v_e$.

The electron beam penetrating the plasma excites a spatially growing electron-plasma wave

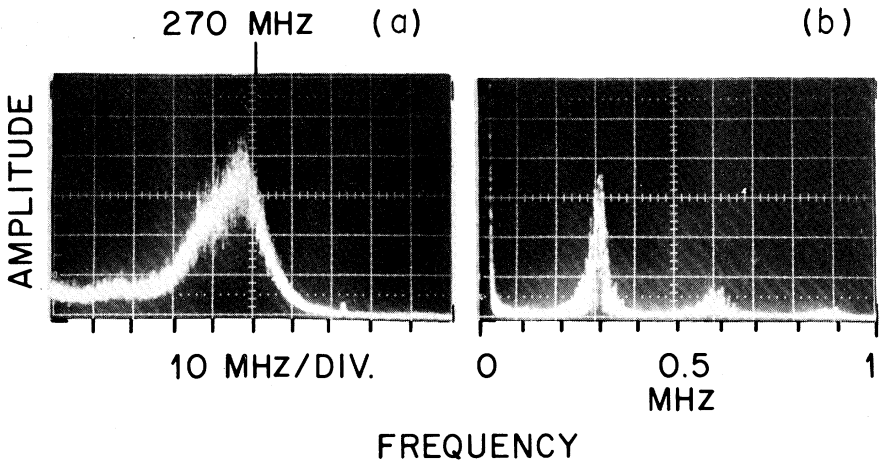

FIG. 1. (a) Decay spectra of the electron-plasma wave. (b) Corresponding ion-acoustic wave. Beam energy = 25 eV and $n_b/n_0 \simeq 0.03$ in both (a) and (b).

with a frequency $\omega_0 \simeq \omega_{pe}$ (electron-plasma frequency ~ 300 mHz) and a width $\Delta\omega \simeq 0.03\omega_0$ as shown in Fig. 1(a). From two-probe spatial-correlation measurements, we have found that the unstable waves propagate at the beam velocity, i.e., with wave number $k_\parallel \simeq \omega_0/u$, and behave like the well-known "bump-on-tail" instability.[4] As the beam strength is increased, $n_b > 0.02n_0$ and $u > 3v_e$, the beam-driven waves reach the level at which they become decay unstable (the backscattering type).[5] This is evidenced by the appearance of a low-frequency component {centered on $\omega_a \sim 300$ kHz [Fig. 1(b)]}. We point out here that the width of the high-frequency spectrum $\Delta\omega$ is an order of magnitude greater than ω_a so that the sideband due to the decay instability cannot be distinguished in the frequency spectrum.

The nonlinear development of the parametric instability is studied by following the space-time evolution of short bursts of small-amplitude ($\delta n/n_0 \sim 1\%$) test ion-acoustic waves. These are launched by modulating the potential between "driver" and "target" chambers at a time $t = 0$, before the large-amplitude negative potential is applied to the driver plasma in order to extract the electron beam [see top trace of Fig. 2(b)]. In Fig. 2(a), the top two traces show density perturbations associated with the wave bursts at times $t = 50$ and 60 μsec after launching, which propagate into the test plasma in the absence of the electron beam. From the relative displacements of test-burst peaks, the ion-acoustic speed is obtained. The negative potential is applied at time $t = 65$ μsec, causing the electron beam to penetrate the test plasma almost instantaneously [(plasma length)/$u < 0.1$ μsec]. Thus traces for $t > 65$ μsec follow wave propagation in the unstable regime. The electron beam excites coupled large-amplitude ion-acoustic and electron-plasma waves[6] (see traces at $t = 70$ and 80 μsec). The original ion-acoustic wave burst acts as a trigger for the instability and locks the initial phase of the unstable wave. (This phase locking enables us to use signal-sampling processing.) The peak-to-peak levels of the low-frequency perturbation reach 20% of n_0 and almost independently of the beam velocity. If the electron beam is turned off at time $t = 105$ μsec, the electron-plasma wave damps away rapidly (no detectable high-frequency signal is measured at 110 μsec), while the ion-acoustic wave, which has a low damping rate, persists for a long time while showing a rapid change in wavelength [last three traces in Fig. 2(a)].

The intensity profile of the electron-plasma wave in Fig. 2(a) (labeled by HF) reveals that the intensity is always at maximum when the ion-acoustic perturbation has a minimum density. Figure 2(b) shows the evolution in time, at a fixed spatial location ($x = 15$ cm from the mesh grid), of the density perturbation and the high-frequency wave intensity. Again it is noted that the electron-plasma wave intensity is largest at the ion-acoustic density minima. This figure also illustrates that the electron-plasma wave intensity reaches a stationary level within a short time (the beam filling time; see inset). Thereafter it grows together with the ion-acoustic burst to a new level, more than an order of magnitude larger than the first.

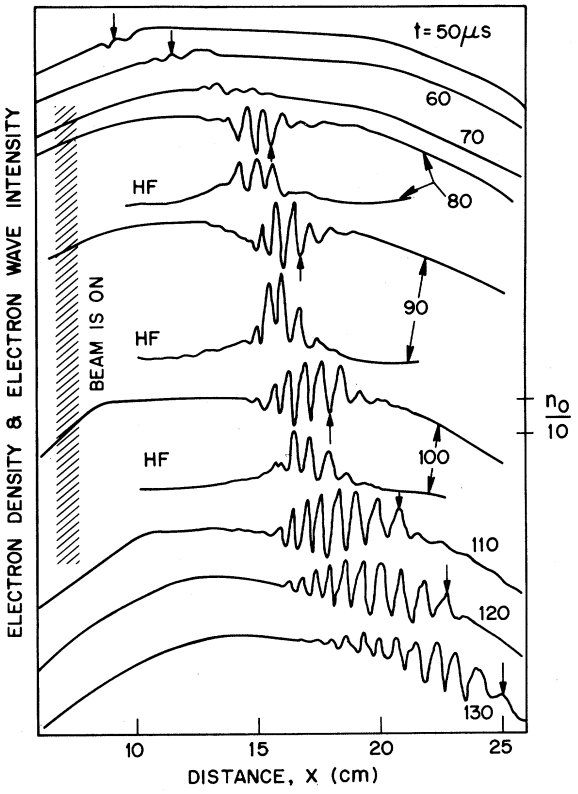

(a)

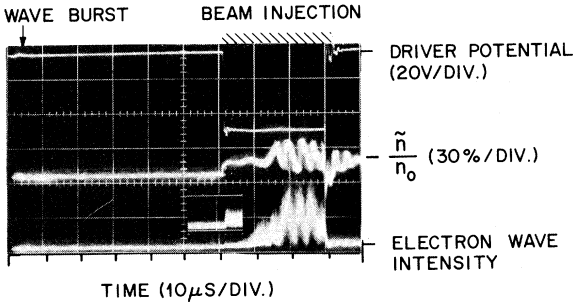

(b)

FIG. 2. (a) Electron density (wave intensity) versus distance for different times after launching of the test wave burst. HF labels the electron-plasma wave intensity and the shaded region on the left corresponds to the duration of the electron-beam injection. The sets of arrows (up or down) identify the constant wave phases. (b) Time evolution of the density perturbation (middle trace) and the high-frequency wave intensity (bottom trace) at fixed location $x = 15$ cm. Top trace shows the beam pulse. Beam energy = 50 eV and $n_b/n_0 \simeq 0.05$ in both (a) and (b).

The above observations demonstrate a completely new feature of the wave interaction. Instead of the simple model, which views the unstable electron-plasma wave as a "pump" feeding energy to the decay products, we find that the convection of the electron-plasma waves is reduced by wave trapping in large-amplitude acoustic perturbations; as a result, the electron-plasma wave interacts with the electron beam for longer time and is enhanced. The wave number and direction of propagation of the electron-plasma wave mode are obtained by measuring the signal correlation function between two probes, as a function of the distance between them during a time interval (0.1 μsec) longer than ω_0^{-1} but shorter than ω_a^{-1}. When a $\pi/2$ phase shift is introduced into one of the probe signals, the correlation is found to decrease, indicating that the electron-plasma mode is a standing wave in the beam direction [see Fig. 3(a)]. Its wave-number component $k_\parallel$ along the beam axis turns out to be one half of the ion-acoustic wave number k_a. It follows that the electron-plasma mode is phase

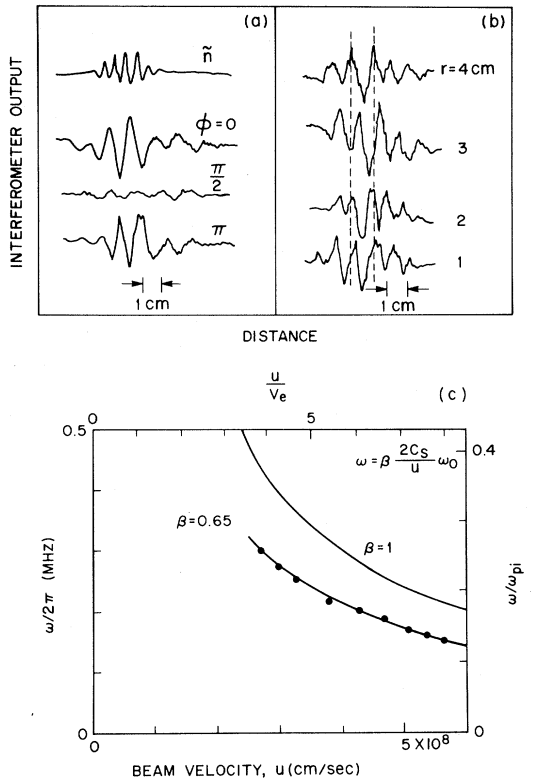

FIG. 3. (a) Typical interferometer output (for different phase shift of the reference signal) of the parallel electron-plasma wave. (b) Interferometer output at different radial locations. Beam energy = 30 eV and $n_b/n_0 \simeq 0.05$. Interferometer bandwidth = 5 MHz in both (a) and (b). (c) Ion-acoustic frequency as a function of the beam velocity for $\beta = 0.65$ and 1.0. Dots are experimental points.

locked or "trapped" within the ion-acoustic troughs, and propagates at the ion-acoustic mode velocity, instead of the phase velocity $\sim u$. In addition, probe measurements at right angles to the beam axis (radial direction) reveal that, while the ion-acoustic wave is a plane wave, the electron-plasma wave consists of modes which are distributed in a range $0 < k_\perp < (\frac{1}{2} - \frac{1}{4})k_\parallel$ in the perpendicular direction. The maximum $k_\perp$ is determined by the radial correlation length observed in Fig. 3(b).[7]

The phase velocity of the locked ion-acoustic mode is slower than the ion-acoustic speed C_s in the unperturbed plasma. The set of three arrows (pointing upward) in the middle of Fig. 2(a) identifies the constant wave phase showing that the phase velocity is $0.6C_s$ during the time when the beam is on. We interpret this decrease of the phase velocity in terms of the ponderomotive force.[8] The ponderomotive pressure should reduce the electron kinetic pressure, since the intensity of the electron-plasma wave is large at the trough of the low-frequency density perturbation. With the inclusion of the ponderomotive force, the wave equation for the ion-acoustic modes takes the form[9]

$$\frac{\partial^2 \tilde{n}}{\partial t^2} - C_s{}^2 \frac{\partial^2 \tilde{n}}{\partial x^2} - \frac{1}{16\pi M} \frac{\partial^2 E_\parallel{}^2}{\partial x^2} = 0, \qquad (1)$$

where $\tilde{n}$ is the density perturbation (measured from density minimum) and $E_\parallel$ is the axial high-frequency field. Phenomenologically, a relation between $\tilde{n}$ and $E_\parallel$ can be expressed as

$$E_\parallel{}^2/16\pi = -\alpha T_e \tilde{n}, \qquad (2)$$

where α is a coefficient. Combining (1) and (2) yields a modified phase velocity $v_p = (1-\alpha)^{1/2} C_s$. Using the observed ratios $v_p/C_s = 0.6$ and $\tilde{n}_{max}/n_0 \approx 0.2$, one obtains the estimate $E_\parallel \sim 40$ V/cm ($E_\parallel{}^2/16\pi n_0 T_e \approx 0.1$). (The probe calibrated at the plasma frequency in a plasma-filled capacitor indicates that $E_\parallel$ is several times 10 V/cm.) With use of the ratio $k_\perp/k_\parallel$, the corresponding value for $E_\perp$ should range between 10 and 20 V/cm. Another check is provided by the frequency ω_a of the ion-acoustic mode. Using the observed relationships $k_a = 2k_\parallel$ and $\omega_0 \simeq k_\parallel u$, we calculate that $\omega_a \equiv k_a v_p = 2C_s \omega_0 (1-\alpha)^{1/2}/u$. A plot of this relationship is shown in Fig. 3(c) for $u < 8v_e$ and $n_b/n_0 \simeq 0.05$. The above relation which takes the decrease of the phase velocity, $\beta \equiv (1-\alpha)^{1/2} = 0.65$, into account fits the experimentally observed frequency.

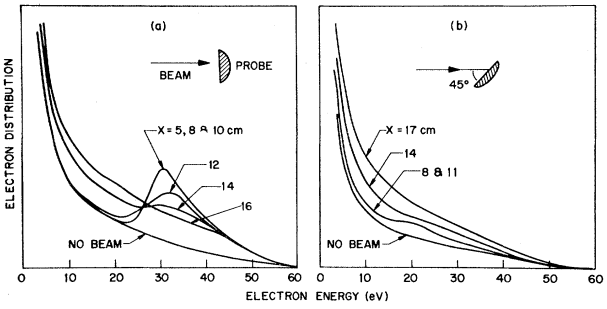

FIG. 4. Electron energy distribution at different locations from the beam entrance for probe surface (a) normal to the beam and (b) at 45 deg to the beam. We observe that the electron-plasma wave has the largest amplitude between $x = 11$ and 14 cm. The "no-beam" curves apply to all distances.

The presence of large-amplitude electric fields, $E_\parallel$ and $E_\perp$, suggests that wave scattering of the electron beam perpendicularly to (as well as along) the axis should occur. This is confirmed by differentiated plane Langmuir-probe current measurements, which yield a value of the electron energy component perpendicular to the probe surface. The beam distribution parallel to the injection direction, Fig. 4(a), is unchanged before the instability takes place, $x < 13$ cm. The beam energy is seen to spread towards the lower-energy side as it enters the unstable region. The "bump-on-the-tail" distribution completely disappears within 3 cm (three electron-plasma wavelengths) following interaction with the unstable high-frequency waves. Figure 4(b) on the other hand shows that the tail of the electron energy distribution measured by probes tilted at 45 deg with respect to the original beam directions increases at the locations where the beam "bump" in the parallel distribution disappears. The maximum perpendicular energy is comparable to the original beam energy. This fact indicates that the high-frequency component $E_\perp$ scatters the beam electrons at an angle to the beam axis, presumably via the usual inverse Landau-type wave-particle entrainment process. We note also that the magnitude of $E_\perp$ necessary to accelerate the beam within a few wavelengths to the energies shown here is consistent with our estimates for $E_\perp$ above.

In conclusion, the nonlinear evolution of the electron-beam-excited backscattering decay process is shown to involve large density fluctuations ($\delta n/n_0 = 20\%$), which cause the trapping of the electron-plasma waves by the ion-acoustic wave.

As the amplitudes of the electron-plasma waves grow they scatter the beam electrons causing the nonlinear instability to saturate and finally quench.

The authors acknowledge discussions with A. Hasegawa, K. Mima, and K. Nishikawa and appreciate the technical support provided by P. J. Casale.

[1]L. Thode and R. N. Sudan, Phys. Rev. Lett. 30, 732 (1973).

[2]A. S. Bakai, E. A. Kornilov, and M. Krivoruchko, Pis'ma Zh. Eksp. Teor. Fiz. 12, 69 (1970) [JETP Lett. 12, 49 (1970)]; R. R. Parker and A. L. Throop, Phys. Rev. Lett. 31, 1549 (1973); B. H. Quon, A. Y. Wong, and B. H. Ripin, Phys. Rev. Lett. 32, 406 (1974).

[3]R. J. Raylor, K. R. MacKenzie, and H. Ikezi, Rev. Sci. Instrum. 43, 1675 (1972).

[4]J. H. Malmberg and C. B. Wharton, Phys. Fluids 12, 2600 (1969); C. Roberson, K. W. Gentle, and P. Nielson, Phys. Rev. Lett. 26, 266 (1971); W. Carr, D. Boyd, H. Lin, G. Schmidt, and M. Seidl, Phys. Rev. Lett. 28, 662 (1972).

[5]V. N. Oraevskii and R. Z. Sagdeev, Zh. Tek. Fiz. 32, 1291 (1962) [Sov. Phys. Tech. Phys. 7, 955 (1963)]; R. P. H. Chang and M. Porkolab, Phys. Fluids 13, 2766 (1970).

[6]These high-frequency signals are detected by a small double probe which couples to the external circuit through a transformer. By checking the directivity and sensitivity we confirmed that the probe detects the electric field. The resonant decoupling which may occur at the plasma frequency is suppressed by choosing a small probe-wire size comparable to the Debye length.

[7]A simple geometric analysis of the dispersion relations indicates that all electron-plasma waves distributed in k space participate in excitation of the parametric instability only when k_a is along the beam and equals $2\omega_0/u$. Therefore, the observed ion-acoustic wave is the most unstable mode.

[8]L. D. Landau and E. M. Lifshitz, *Electrodynamics of Continuous Media* (Pergamon, New York, 1960), Eq. (15.14).

[9]A. Hasegawa, Phys. Rev. A 1, 1746 (1970); V. E. Zakharov, Zh. Eksp. Teor. Fiz. 62, 1745 (1972) [Sov. Phys. JETP 35, 908 (1972)].

Turbulent Lifetimes in Mirror Machines*

D. E. Baldwin, H. L. Berk, and L. D. Pearlstein
Lawrence Livermore Laboratory, University of California, Livermore, California 94550
(Received 13 January 1976)

A quasilinear model is developed describing the time evolution of a mirror-confined plasma which is unstable to the drift-cyclotron loss-cone mode. Good correlation is obtained with experiments with and without an external stream of cold plasma.

Linear stability analyses of mirror machines with loss-cone ion distributions indicate that current high-density machines are unstable to the drift-cyclotron loss-cone (DCLC) mode with broadband frequency and wave-number spectra.[1,2] With the assumption that the ions are lost in a transit time after scattering into the loss cone, a previous quasilinear treatment predicted the trapped-plasma lifetime to be a few axial bounce periods.[3] This picture has seemingly been contradicted by experiments, as narrow-band spectra and containment times of several hundred bounce periods have been observed.[4,5] Added to this, when a cold-plasma stream is injected, the containment time increases several fold.[6,7]

In this note we show that with refinement the quasilinear picture is indeed consistent with experiment and provides a unified description both with and without plasma stream. The essential modification from past analysis is to observe that mirror plasmas do not necessarily fill the entire containment region of phase space available to them, but can be peaked at pitch angles nearly perpendicular to the magnetic field. Confinement is then improved, both because the unconfined phase-space region is given by $v_\perp^2 < (2q\Phi/M_i + v_\parallel^2)/(R-1)$, and so is reduced if $v_\parallel^2 \lesssim 2q\Phi M_i^{-1}$ (Φ is the ambipolar potential and R the mirror ratio), and because untrapped particles of small $v_\parallel$ at the midplane have a longer transit time. The peaked distribution is maintained by the dominant velocity-space transport processes: electron drag which alters only the particle speed, and turbulent diffusion which affects primarily the perpendicular velocity $v_\perp$. In such cases the scattering time of ion-ion collisions, leading to pitch-angle broadening, is much longer than the first two transport processes, hence ion scattering does not alter the sharply peaked nature of the distribution. If the plasma initially

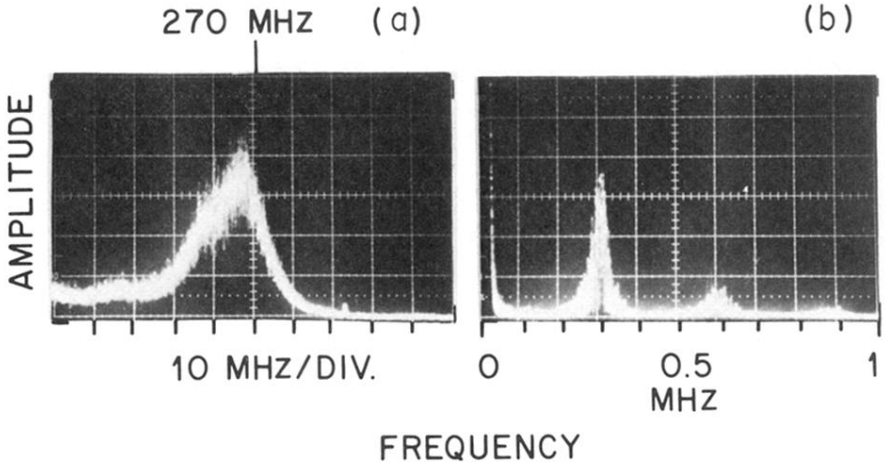

FIG. 1. (a) Decay spectra of the electron-plasma wave. (b) Corresponding ion-acoustic wave. Beam energy = 25 eV and $n_b/n_0 \simeq 0.03$ in both (a) and (b).

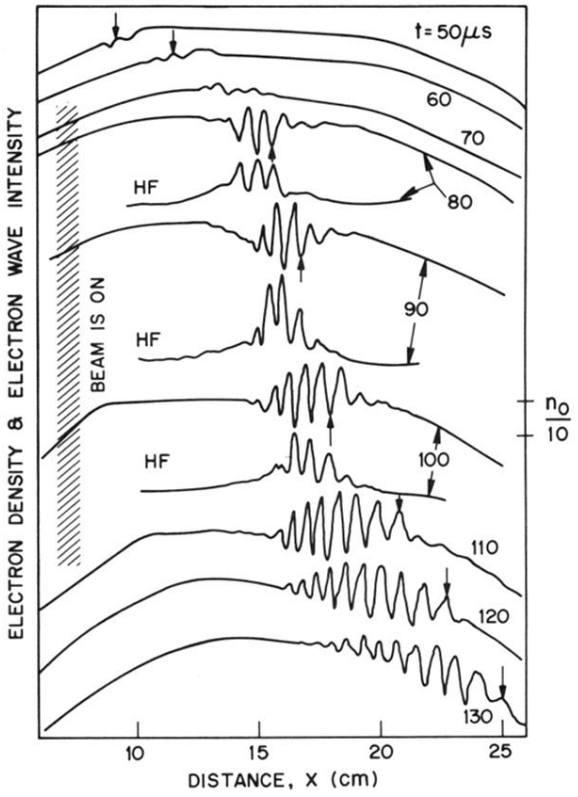

(a)

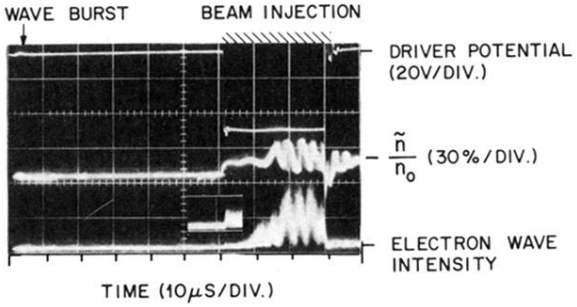

(b)

FIG. 2. (a) Electron density (wave intensity) versus distance for different times after launching of the test wave burst. HF labels the electron-plasma wave intensity and the shaded region on the left corresponds to the duration of the electron-beam injection. The sets of arrows (up or down) identify the constant wave phases. (b) Time evolution of the density perturbation (middle trace) and the high-frequency wave intensity (bottom trace) at fixed location $x = 15$ cm. Top trace shows the beam pulse. Beam energy = 50 eV and $n_b/n_0 \simeq 0.05$ in both (a) and (b).